


## PAPER

[View Article Online](#)  
[View Journal](#) | [View Issue](#)Cite this: *Digital Discovery*, 2025, 4, 979

## Automating stochastic antibody–drug conjugation: a self-driving lab approach for enhanced therapeutic development†

Liam Roberts,<sup>a</sup> Matthew E. Reish,<sup>a</sup> Jerrica Yang,<sup>a</sup> Wenyu Zhang,<sup>a</sup> Joshua S. Derasp<sup>\*a</sup> and Jason E. Hein<sup>†a</sup>  <sup>abcd</sup>

Antibody–drug conjugates (ADCs) have become a promising cancer treatment over the past two decades due to their on-target drug-release capabilities. However, labor-intensive manual conjugations currently limit the throughput of ADC synthesis. Herein, we introduce a Self-Driving Lab (SDL) for automated stochastic antibody–drug conjugation and characterization. The robotic platform performs conjugations and determines drug to antibody ratios from chromatography data, enabling the production of target ADCs iteratively in a closed loop. Our SDL establishes a robust foundation for increasing ADC production throughput and accelerating the development of cancer therapeutics.

Received 9th November 2024  
Accepted 21st February 2025

DOI: 10.1039/d4dd00363b

[rsc.li/digitaldiscovery](https://rsc.li/digitaldiscovery)

## Introduction

Cancer remains a significant global health issue, resulting in 10 million deaths in 2020 and ranking as the second most common cause of mortality worldwide.<sup>1</sup> Among various treatment strategies, antibody–drug conjugates (ADCs) have emerged as a highly promising category of cancer therapies.<sup>2,3</sup> By directly delivering drugs to cancer cells, the antibody minimizes toxicity to healthy tissues.<sup>2,3</sup>

Several methods facilitate the attachment of linker-bound drugs (drug-linkers) to the antibody's amino acid residues.<sup>4</sup> Site-specific conjugation often uses artificially inserted amino acid residues to achieve uniform attachment of drug-linkers.<sup>4</sup> In contrast, stochastic conjugation uses the antibody's native lysine or cysteine residues, resulting in a non-uniform binding of drug-linkers.<sup>4</sup> Stochastic cysteine conjugation has proven effective for five of the eleven FDA-approved ADCs and many ADCs that are currently in clinical trials.<sup>5,6</sup>

IgG1 antibodies contain 8 key cysteine residues which are present as interchain disulfide bridges.<sup>4</sup> The stochastic reduction of these bonds exposes the nucleophilic thiols which can then be reacted with a maleimide drug-linker containing a chemotherapeutic payload.<sup>4</sup> The average drug-to-antibody ratio (DAR) is a key parameter that influences efficacy and toxicity of the resulting ADC.<sup>5–7</sup> However, the laborious nature of

manual antibody conjugation is a bottleneck to ADC screening and development.<sup>8</sup> This bottleneck is particularly evident because ADC precursors can be produced at high throughput through modern drug and antibody screening methods.<sup>9–11</sup>

Previous studies have focused on optimizing isolated aspects of the conjugation and characterization protocols for stochastic ADC production.<sup>12–14</sup> For example, Endo *et al.* employed flow reactors to accelerate reduction and conjugation reactions,<sup>12</sup> while Yang *et al.* introduced an automated buffer exchange system to streamline ADC preparation for mass spectrometry analysis.<sup>13,14</sup> Goyon *et al.* developed a rapid characterization approach using online 2D and 4D liquid chromatography.<sup>14</sup> Despite these advancements, the development of a fully autonomous platform capable of synthesizing ADCs with precise drug-to-antibody ratios (DAR), a key developmental parameter, remains a significant challenge. A platform with integrated feedback control, enabling on-the-fly testing and optimization of experimental conditions, would represent a major advancement for the field. Further, reliable synergy between data extraction algorithms and hardware would drastically improve the ability to design ADCs with precise drug-to-antibody ratio (DAR) outputs, ultimately enhancing the production of targeted therapeutics.

In this work, we introduce an automated robotic platform for the synthesis of stochastic antibody–drug conjugates (Fig. 1). This platform integrates a custom liquid handling system for performing the reactions with hydrophobic interaction chromatography-high-performance liquid chromatography (HIC) for drug-to-antibody ratio (DAR) characterization. We developed an algorithm capable of extracting the average DAR from chromatographic data, streamlining the analysis process. Additionally, our platform optimizes conjugation conditions providing access to ADCs with precise DARs. Together, these

<sup>a</sup>Department of Chemistry, The University of British Columbia, Vancouver, BC V6T 1Z1, Canada. E-mail: [jhein@chem.ubc.ca](mailto:jhein@chem.ubc.ca); [jderasp@chem.ubc.ca](mailto:jderasp@chem.ubc.ca)<sup>b</sup>Department of Chemistry, University of Bergen, Norway<sup>c</sup>Acceleration Consortium, University of Toronto, Toronto, ON, Canada<sup>d</sup>Telescope Innovations Corp., Vancouver, BC, Canada† Electronic supplementary information (ESI) available. See DOI: <https://doi.org/10.1039/d4dd00363b>

advancements demonstrate a proof-of-concept for significantly increasing the throughput of ADC production, with potential implications for accelerating cancer therapeutic development.

## Results and discussion

### Conjugation procedure

We began by testing a fully manual workflow to verify that both the chemistry and analytical processes were functioning as expected. This manual execution allowed us to establish a baseline for the conjugation protocol in terms of error rates, analytical precision, and the operational limits of each unit operation. This baseline assessment was critical for identifying potential bottlenecks, ensuring reliable performance of each step—reduction, conjugation, and purification—and confirming that the HIC analysis for drug-to-antibody ratio (DAR) determination was accurate. By understanding the inherent variability and limitations of the manual process, we could subsequently refine the automation, making targeted adjustments to ensure the system operated consistently. The manual workflow also provided a reference point for comparing the performance of the automated platform and guiding optimization efforts during the automation phase.

To generalize our approach, we adopted a standard procedure for stochastic cysteine conjugation as the foundation for automating ADC synthesis (Fig. 2). This process starts with the incubation of an antibody solution with a phosphine-based reductant, tris(2-carboxyethyl)phosphine (TCEP), at 37 °C for 3 hours. The reduction cleaves the disulfide bonds within the antibody, freeing the cysteine thiol groups. After incubation, the reduced antibody solution is passed through a gel-filtration column to remove excess TCEP and other small molecules.

The reduced antibody is then reacted with an excess of maleimide drug-linker, maleimidocaproyl-valine-citrulline-*p*-amino-benzoyloxycarbonyl monomethylauristatin E (vcMMAE),

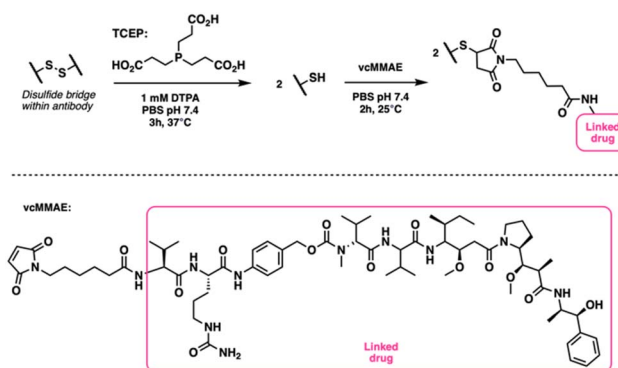


Fig. 2 Schematic of the antibody–drug conjugation procedure. The antibody's interchain disulfide bonds are reduced with TCEP, and a maleimide drug–linker (vcMMAE) is added in excess to conjugate to the thiols and generate an ADC.

at 25 °C for 2 hours. This allows the maleimide groups to covalently attach to the free thiol groups on the antibody. After the conjugation step, the mixture is filtered through another gel-filtration column to remove any unreacted drug-linker, yielding the purified antibody–drug conjugate (ADC). The purified ADC is then analyzed using HIC to determine the DAR. For this study, we used trastuzumab as the antibody and vcMMAE as the drug-linker due to their common use in ADC development.<sup>4–6,15,16</sup>

One of the key challenges in ADC conjugation is that the reactions are typically carried out on a low microliter (μL) scale, which demands highly accurate and precise liquid handling. This is particularly important when transitioning to an automated workflow, as small deviations in liquid handling can significantly affect the outcome of the reaction. To address this, we used dilute solutions during manual experimentation. This approach allowed for the use of larger reagent volumes during

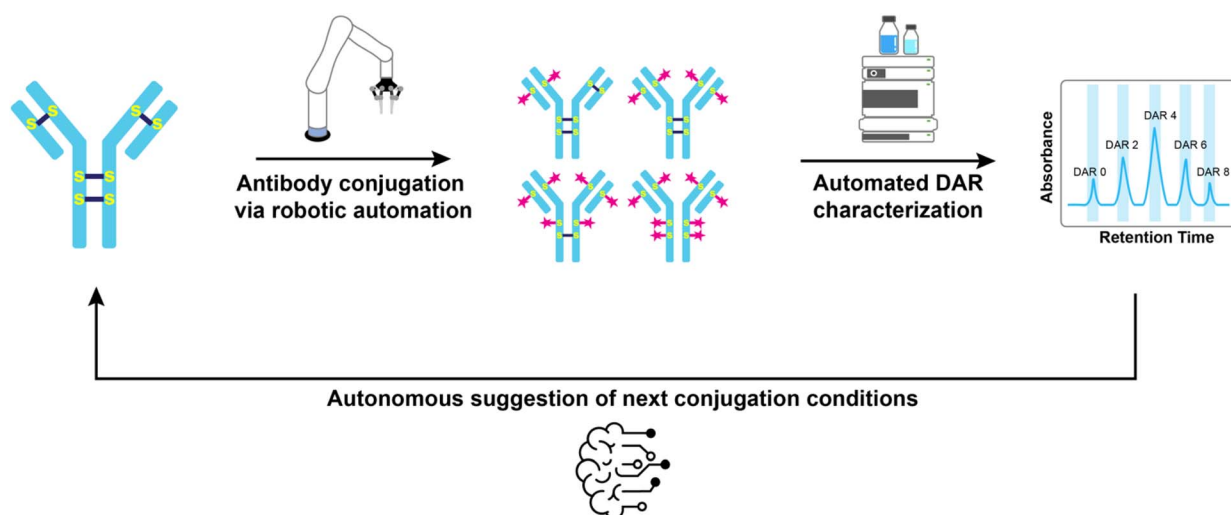


Fig. 1 Self-driving lab for stochastic antibody–drug conjugation. The automated robotic system performs stochastic cysteine conjugation. The distribution of the ADC's DAR species is analysed by HIC, followed by an algorithmic calculation to determine the ADC's average DAR. The platform then suggests alternative conjugation conditions to produce an ADC with the target DAR.



the automation phase, minimizing costs while maintaining feasibility. Through repeated manual conjugations, we verified that the low antibody concentration did not cause significant variability in the ADC's DAR (see ESI Table 3†). Additionally, a crucial post-conjugation step involves removing excess drug-linker to prevent interference with downstream ADC applications. Consequently, the automated system must have a reliable purification protocol to ensure that unreacted drug-linker is effectively removed without compromising the yield or integrity of the ADC.

### Automated conjugation platform

The challenges of precise liquid handling and reliable automated purification were central to our platform development. Managing small reaction volumes with high accuracy and minimizing variability in reagent dispensing were crucial for reproducibility. At the same time, ensuring that our purification system could effectively remove unreacted drug-linker while maintaining high antibody yields was equally important. These technical hurdles shaped our design choices, which aimed to create a robust, modular system capable of performing autonomous ADC synthesis.

Our automated conjugation platform, shown in Fig. 3, was designed with modularity in mind, allowing flexibility in execution and workflow design. At the core of the system is a Kinova Gen 3 robot arm, which transfers samples between the liquid handler, filtration blocks, and other modules.

The robot arm, with its seven degrees of freedom, allows for precise manipulation of micro-scale volumes across the various components. While some modules, such as the IKA thermo-shaker, were easily integrated from commercially available units for temperature control during reactions, key operations like liquid handling and antibody purification required custom in-house solutions (ESI Fig. 3 and 7†).

**Liquid handling challenges and solutions.** Accurate and precise liquid handling represents the first major challenge in automating ADC synthesis, particularly when working with reaction volumes in the 20–40  $\mu\text{L}$  range. While enterprise-level liquid handling systems (e.g., Tecan, Hamilton) can manage such small volumes with high accuracy, they lack the flexibility and hardware/software integration required to build our own autonomous workflow that could incorporate parameter optimization informed by the analytical data without a human in the loop. By taking this flexible automation approach, we were able to reconfigure existing hardware for this new, more challenging application within just a few weeks after iterative refinements, positioning it as a viable alternative to more rigid commercial systems.

Central to this platform was a custom mobile liquid handler, developed in collaboration with Telescope Innovations. This unit is battery-powered, wirelessly operated, and equipped with 3D-printed handles to interface with the robotic arm. Its mobility across the deck, constrained only by the range of the robotic arm, enabled flexible reagent handling and integration into the workflow without requiring manual repositioning.

While the liquid handler performed accurately for larger volumes, early tests showed significant inaccuracies when handling smaller volumes, particularly in the 20–40  $\mu\text{L}$  range, where error rates were around 30% (see Fig. 4 and ESI Table 1,† average error %).

The early performance limitations led us to probe the impact of several parameters including:

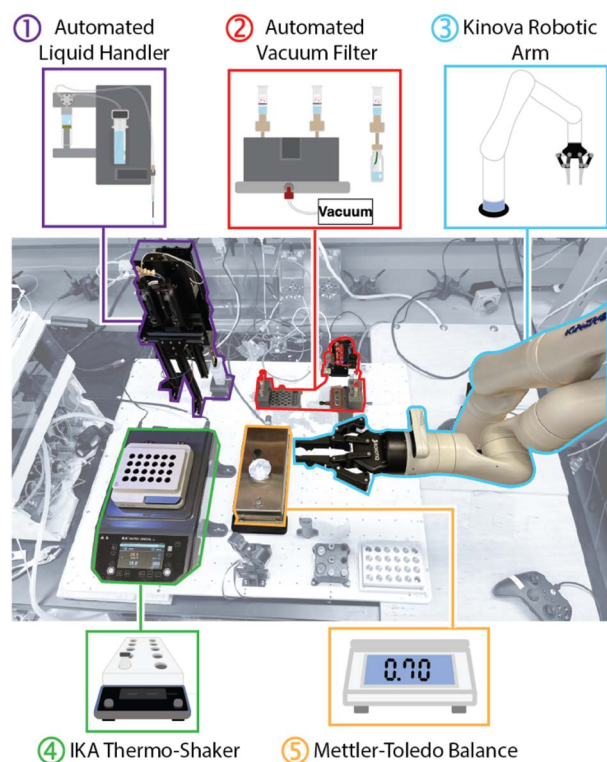


Fig. 3 Overview of automated conjugation deck. (1) A liquid handler comprising a vertically moving needle, a syringe pump, and a solvent reservoir. (2) A vacuum filtration system consisting of a solenoid, a 3D-printed filter block and base, and an IKA Vacstar vacuum pump. (3) A Kinova Gen 3 robot arm with 7 degrees of freedom. (4) An IKA Matrix Delta Orbital Plus thermo-shaker. (5) A Mettler-Toledo WKS204C balance equipped with a custom-built HPLC vial holder. Not highlighted is a custom-built vial capper and cap holder that ensures HPLC vials are sealed during reactions.

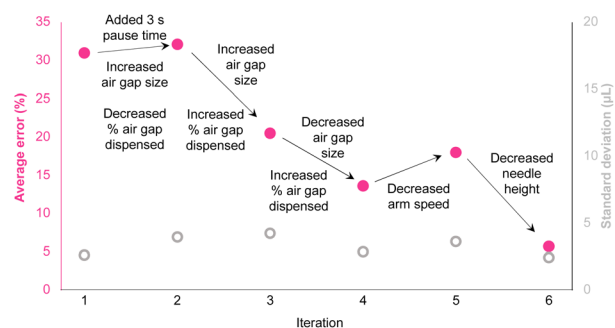


Fig. 4 Liquid handling parameter optimization to reduce average error (pink) and maintain low standard deviation (grey). Variables included air gap size and dispense percentage, pause time to stabilize aspiration, speed of the robotic arm, and the height of the needle after priming. Full parameter details are available in ESI Table 1.†





(A) Airgap size optimization: by varying the size of the airgap used during aspiration, we were able to prevent mixing between the aspirated reagent and the backing solvent. Testing various airgap sizes also allowed us to fine-tune how much air was dispensed with each reagent, ensuring full ejection while minimizing variability.

(B) Aspiration stabilization: we hypothesized that introducing a three-second pause after aspiration could help stabilize the needle, reducing vibrations that could disturb the reagent in the syringe. No significant impact was observed however this change was carried forward as a precautionary measure.

(C) Robotic arm movement: in the same vein, the robotic arm movement could itself potentially impact reagent mixing/airgap mixing during reagent translocation. Although no significant impact on the error was observed, this change was carried through as a precautionary measure.

(D) Needle height adjustment: finally, we adjusted the height of the needle after priming to avoid residual water buildup on the needle guide. This fine-tuning was essential to ensure that each drop of reagent was fully ejected without leaving trace amounts behind that could skew the volumes in subsequent steps.

(E) Gravimetric cross checking and verification: we incorporated an analytical balance (Mettler-Toledo) into the workflow to measure the mass of transferred reagents and enable real-time corrections to reagent volumes (ESI Fig. 15†). By recording the exact mass of solution transferred at each step, the system could dynamically adjust subsequent volumes, ensuring accurate liquid handling despite any small discrepancies in aspiration or dispensing, dramatically increasing the precision of the liquid transfer steps, particularly in the lower microliter range.

**Automated purification challenges and solutions.** The purification process represented a significant challenge, as it required the efficient removal of unreacted drug-linker while maximizing antibody recovery. Our goal was to develop a method capable of achieving at least 50% antibody recovery while limiting drug-linker carryover to less than 1%. Inspired by Andris *et al.*'s site-specific conjugation platform,<sup>17</sup> we incorporated 0.5 mL 40K Zeba spin desalting columns into our vacuum-based system. However, these columns were originally designed for manual centrifugation, so adapting them for fully automated operation necessitated several adjustments.

To address these challenges, we developed custom-built filtration modules (Fig. 5 and ESI Fig. 7†) that utilized vacuum-driven gel-filtration columns. A mobile vacuum filtration block was designed to integrate with the robotic arm and liquid handler. This enabled the initial washing of the stabilizing solution from the column into waste vials. The robot arm then moves the filtration block to the sample vials to conduct the filtration and acquisition of the desired sample, all in the absence of manual intervention. However, achieving consistent yields from the small volumes typical in ADC synthesis proved particularly difficult. Early tests revealed substantial variability in filtration efficiency, with yields fluctuating based on factors such as vacuum strength, filtration time, and tubing geometry.

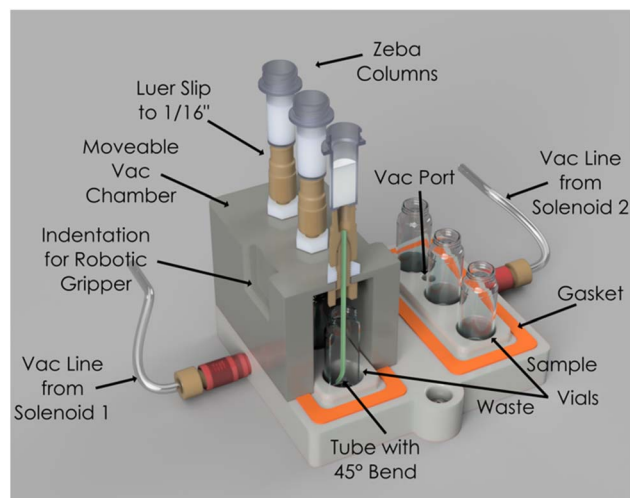


Fig. 5 Schematic of the custom vacuum filtration module for automated antibody purification. The system integrates Zeba spin columns into a movable vacuum chamber, controlled via solenoid-actuated vacuum lines for precise filtration.

Furthermore, the air flow from the tubing line was found to splatter the sample along the walls of the vial and tubing line. This is a particular problem on such small scale as it impedes subsequent sampling as well as introducing contamination issues on the tubing line when moving from the stabilizing solution filtration to the sample filtration. These inconsistencies led us to systematically optimize the process by iteratively testing and refining various configurations. Critical adjustments—including modifying vacuum strength and tubing geometry—were essential in minimizing liquid splatter and maintaining sample integrity.

During the optimization process, we tested several key parameters to improve filtration efficiency, including the inner diameter (ID) of the tubing, vacuum strength, and vacuum duration (Fig. 6, ESI Fig. 8b, c and Table 2†). Initial trials using a 0.03 inch ID tube at vacuum strengths of 400 mbar and 600 mbar for 30 and 60 seconds, respectively, resulted in high antibody yields but caused excessive liquid splatter, compromising sample integrity. In an attempt to resolve this, we tested narrower tubing (0.01 inch and 0.02 inch IDs), which successfully eliminated splatter but reduced antibody recovery.

Ultimately, we reverted to the 0.03 inch ID tubing and modified its geometry by bending the tube to direct liquid flow toward the side of the waste vial (ESI Fig. 8c†). This adjustment successfully prevented splatter. Using this configuration at 600 mbar for 60 seconds, we achieved optimal antibody recovery while minimizing drug-linker carryover, ensuring the integrity of the final product. These refinements allowed us to address the primary challenges of purification—efficient filtration and consistent antibody recovery from small sample volumes.

### DAR determination algorithm

The average drug-to-antibody ratio (DAR) is a pivotal factor in determining the therapeutic efficacy and safety profile of



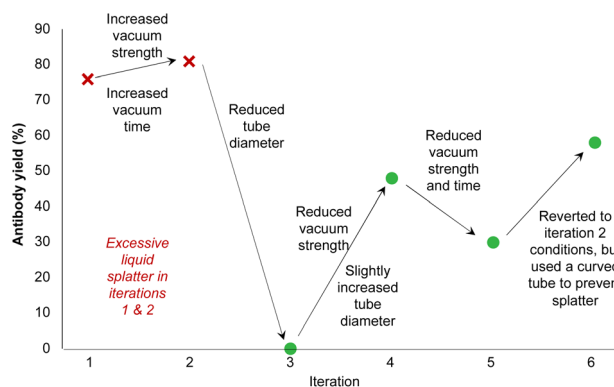


Fig. 6 Vacuum filtration parameter optimization to increase antibody yield. Variables include the inner diameter of the tubing, vacuum strength and time, and the geometry of the tube. Full parameter details are available in ESI Table 2.†

antibody–drug conjugates (ADCs). Even slight deviations in the DAR can significantly shift the balance between potency and toxicity, impacting both clinical outcomes and patient safety.<sup>5–7</sup> Stochastic cysteine conjugation inherently results in a heterogeneous mixture of ADCs, each displaying a distinct level of drug attachment, known as DAR species (typically DAR 0, 2, 4, 6, or 8) (Fig. 7a)<sup>4</sup> where variability arises from the reduction of native interchain disulfide bonds to expose two reactive thiols, enabling conjugation with excess drug-linker molecules. The prevalence of even-numbered DAR species reflects this dual-

thiol reactivity.<sup>8</sup> However, inherent heterogeneity in conjugation underscores the critical need for precise DAR characterization, as even minor discrepancies in DAR can drastically alter the therapeutic window, affecting both the efficacy and tolerability of the resulting ADCs. Achieving consistent, optimized DAR is thus essential for advancing the next generation of targeted cancer therapies.

Our automated platform leverages HIC to separate and quantify DAR species based on their hydrophobicity profiles. An increase in the conjugated drug load correlates with increased hydrophobicity, which is readily resolved in chromatographic analysis. The resulting chromatograms are rich in information yet interpreting them accurately has traditionally been a labour-intensive task. Here, we automate both the analytical acquisition and data interpretations process with a robust algorithm that dynamically assigns DAR values, significantly enhancing the throughput and precision of ADC characterization.<sup>18,19</sup>

The DAR determination algorithm replicates the nuanced decision-making process a skilled researcher would use when interpreting HIC data, translating it into a streamlined digital workflow (see ESI† for algorithm details).<sup>18,19</sup> Initially, it assigns DAR species based on the elution order of dominant peaks (Fig. 7a). However, the complexity of the chromatogram—often populated with minor peaks from degradation products or residual unreacted drug-linker—can lead to erroneous DAR assignments if based purely on elution sequence.<sup>20–22</sup> To circumvent this challenge, our algorithm integrates ultraviolet (UV) absorbance analysis at 280 nm (tryptophan and tyrosine

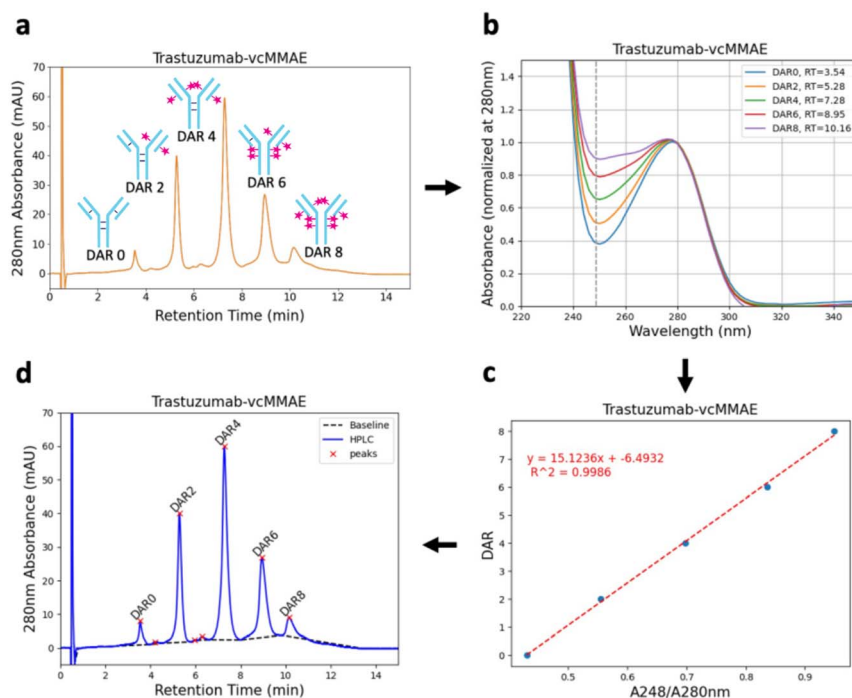


Fig. 7 Schematic of the DAR determination algorithm workflow, integrating HIC peak assignment, UV absorbance analysis, and linear correlation to accurately quantify drug-to-antibody ratios for ADCs. (a) Raw HIC chromatograms, (b) UV-Vis absorption spectra recorded *via* DAD used to extract absorbance difference between peaks (c) linear relationship for key  $A_{248}/A_{280}$  ratios, (d) final process chromatogram with auto-assigned DAR numbers.



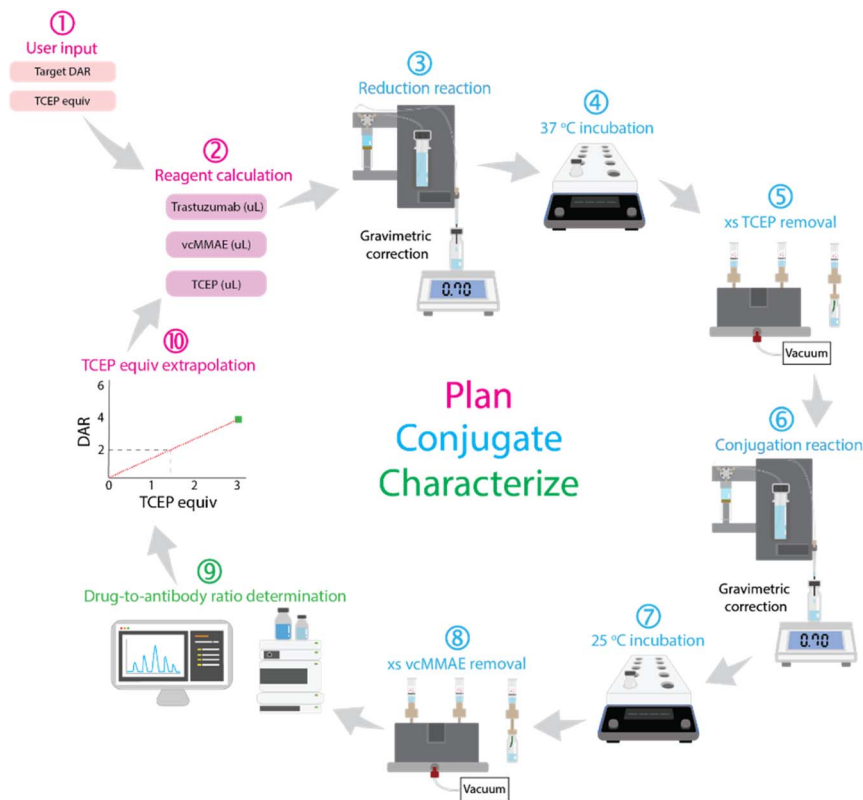


Fig. 8 Schematic of the autonomous workflow for antibody–drug conjugation, integrating automated reduction, conjugation, purification, and real-time DAR analysis with iterative optimization.

residues in antibody) and 248 nm (drug-linker vcMMAE) to validate each assignment (Fig. 7b).<sup>23</sup> As the number of conjugated vcMMAE molecules increases, the absorbance at 248 nm rises linearly.<sup>18</sup> After correlating the ratio of  $A_{248}/A_{280}$  absorbance with the degree of conjugation, the algorithm applies a linear regression model to confirm the accuracy of DAR assignments, ensuring that only peaks with a strong linear relationship ( $R^2 > 0.99$ ) are accepted (Fig. 7c).

Notably, this step relies on the presence of different absorbance maxima between the drug-linker and the antibody. However, similar DAR determination strategies, such as UV-Vis spectroscopy, have been employed manually with differences as small as 10 nm.<sup>23,24</sup> Furthermore, a peak deconvolution algorithm is included in our workflow to enable its use in settings with difficult HIC separations, a known problem in ADC developments. This provides a broadly applicable automated workflow for DAR determination as a key feature of our platform.

To further refine accuracy, the algorithm automatically excludes peaks that deviate from the expected linear correlation, which are typically associated with degradation products or unbound drug-linker. This iterative reassignment ensures that only the most reliable peaks contribute to the final weighted DAR calculation. The result not only enhances the precision of DAR determination but also seamlessly integrates into our autonomous conjugation workflow, providing real-time feedback for optimizing reaction conditions.

After peak assignment, the algorithm integrates the peak areas using tangential skims (Fig. 7d and ESI Fig. 17†) and calculates the weighted average DAR of the ADC (using the equation in ESI Fig. 12†).<sup>18</sup> A limitation of the algorithm is that it requires at least three DAR peaks to confirm the assignments, though this is typically not an issue given the broad distribution of DAR species produced through stochastic conjugation.<sup>8,25</sup> All HIC data in this project were analyzed using this algorithm, which was validated across a wide range of average DAR values, from 1.97 to 6.60 (ESI Fig. 18†). This fully automated approach to DAR analysis exemplifies the power of digital innovation in streamlining ADC development, paving the way for faster and more efficient synthesis of targeted cancer therapeutics.

### Autonomous conjugation workflow

Manual synthesis of an ADC with a specific drug-to-antibody ratio (DAR) involves a lengthy, iterative process where researchers adjust reaction conditions based on the outcomes of initial conjugations.<sup>26</sup> This process relies on assumed predictable linear correlation between DAR and the concentration of reducing agents, such as tris(2-carboxyethyl)phosphine (TCEP). Our automated system replicates this decision-making process, transforming it into a fully autonomous workflow.

In our platform, the process begins with the user specifying the target DAR and reaction conditions, including the required TCEP equivalents (Fig. 8(1)). The system then calculates the



appropriate reagent volumes (Fig. 8(2)) and initiates the conjugation sequence. Once the reaction is complete, the resulting ADC is analyzed using HIC, with our algorithm determining the average DAR (Fig. 8(9)). If the measured DAR does not match the target, the system constructs a zero-intercept linear relationship between the DAR and TCEP concentration. This enables the platform to dynamically adjust TCEP equivalents for subsequent iterations (Fig. 8(10)), iteratively refining conditions to converge on the desired DAR.

The key innovation of our workflow lies in its integration of real-time, data-driven decision-making. The system continuously adjusts reaction parameters based on analytical feedback, rather than relying on predefined conditions. This adaptability creates a continuous feedback loop where reaction planning, execution, and characterization inform one another, significantly reducing human intervention and enhancing reproducibility.

### Application to trastuzumab and vcMMAE conjugation

To validate the platform, we applied it to the synthesis of ADCs using trastuzumab and the drug-linker vcMMAE. First, we assessed the platform's ability to produce and characterize an ADC without specifying a target DAR. Using an arbitrary amount of TCEP, the system successfully synthesized an ADC with a DAR of 3.85 (ESI Fig. 19a†), confirming the accuracy of the end-to-end process including synthesis, purification, and characterization.

Next, we evaluated the closed-loop workflow for producing an ADC with a target DAR of 6. In the initial attempt, the system synthesized an ADC with a DAR of 3.39 (ESI Fig. 19b†). Based on this result, the system established a linear correlation between DAR and TCEP equivalents and adjusted the concentration accordingly for the next iteration. This adjustment produced an ADC with a DAR of 6.6 (ESI Fig. 19c†), which slightly exceeded the target due to a liquid handling error—9.9 TCEP equivalents (43.1  $\mu\text{L}$ ) were added instead of the intended 8.1 (35.2  $\mu\text{L}$ ). These results highlight the need for further refinement of the liquid handling module to improve precision at low dosing volumes which are on-going in our laboratory (see ESI† for further discussion).

In summary, our autonomous workflow successfully demonstrated its ability to optimize ADC synthesis iteratively. However, improving the precision of the liquid handling system will be essential to achieve consistent target DARs within a narrow margin of error ( $\pm 0.2$  DAR).

## Conclusion

In this work, we developed a self-driving laboratory (SDL) platform that autonomously performs stochastic antibody–drug conjugate (ADC) synthesis and precise drug-to-antibody ratio (DAR) characterization. The automated workflow integrates modular hardware components for stirring, temperature control, sample transfer, and purification, along with a custom liquid handling unit and an in-house developed DAR determination algorithm. This highly flexible system was validated

using stochastic cysteine-based conjugations—one of the most commonly employed methods for ADC production.

The modular design of the platform will allow for straightforward adaptation, such as running optimizations of the conjugation conditions, or broadening to other settings such as lysine-based conjugations, with minimal reconfiguration. By leveraging real-time data feedback and iterative optimization, the system significantly reduces the manual effort and time typically required for ADC synthesis.

Looking ahead, our efforts will focus on enhancing the precision of the liquid handling module to reliably achieve target DARs with tighter tolerances. This advancement will further optimize the platform's capability to produce ADCs with consistent therapeutic profiles. Ultimately, our SDL prototype demonstrates the potential to streamline the production of ADCs, thereby accelerating the development of next-generation cancer therapies. This work lays the foundation for broader applications of autonomous systems in pharmaceutical development, driving both efficiency and innovation in the field.

## Data availability

The hardware design files are available at <https://gitlab.com/heingroup/adc-automation-hardware>. The automation system and DAR determination algorithm are available at <https://gitlab.com/heingroup/adc-automation>. A combined dataset DOI is available at <https://doi.org/10.5281/zenodo.14902831>.

## Author contributions

Liam Roberts: conceptualization, methodology, investigation, analysis, writing – original draft, visualization. Matthew E. Reish: hardware development, data curation, formal analysis, validation, writing – review & editing. Jerica Yang: software development, methodology, investigation. Wenyu Zhang: software development, data analysis, algorithm development, validation, writing – review & editing. Joshua S. Derasp: project administration, experimental design, methodology, writing – review & editing. Jason E. Hein: conceptualization, supervision, project administration, funding acquisition, writing – review & editing, visualization. All authors have read and approved the final version of the manuscript.

## Conflicts of interest

There are no conflicts to declare.

## Acknowledgements

The authors acknowledge Paloma Prieto and Dr Ekaterina Trushina for their insightful guidance and conversation during the preparation of this manuscript. Financial support for this work was provided The University of British Columbia, the Canada Foundation for Innovation (CFI-35883, CFI-44843), the Natural Sciences and Engineering Research Council of Canada (NSERC; RGPIN-2021-03168, Discovery Accelerator





Supplement), and the Canada First Research Excellence Fund (CFREF2022-00042).

## Notes and references

- 1 H. Sung, J. Ferlay, R. L. Siegel, M. Laversanne, I. Soerjomataram, A. Jemal and F. Bray, *Ca-Cancer J. Clin.*, 2021, **71**, 209–249.
- 2 S. C. Alley, N. M. Okeley and P. D. Senter, *Curr. Opin. Chem. Biol.*, 2010, **14**, 529–537.
- 3 J. Z. Drago, S. Modi and S. Chandarlapaty, *Nat. Rev. Clin. Oncol.*, 2021, **18**, 327–344.
- 4 H. Yao, F. Jiang, A. Lu and G. Zhang, *Int. J. Mol. Sci.*, 2016, **17**, 194.
- 5 L. Gauzy-Lazo, I. Sassoon and M.-P. Brun, *SLAS Discovery*, 2020, **25**, 843–868.
- 6 H. Maecker, V. Jonnalagadda, S. Bhakta, V. Jammalamadaka and J. R. Junutula, *mAbs*, 2023, **15**, 2229101.
- 7 T. D. Nguyen, B. M. Bordeau and J. P. Balthasar, *Cancers*, 2023, **15**, 713.
- 8 M. M. C. Sun, K. S. Beam, C. G. Cervený, K. J. Hamblett, R. S. Blackmore, M. Y. Torgov, F. G. M. Handley, N. C. Ihle, P. D. Senter and S. C. Alley, *Bioconjugate Chem.*, 2005, **16**, 1282–1290.
- 9 P. Szymański, M. Markowicz and E. Mikiciuk-Olasik, *Int. J. Mol. Sci.*, 2012, **13**, 427–452.
- 10 Y. Wang, R. Jin, B. Shen, N. Li, H. Zhou, W. Wang, Y. Zhao, M. Huang, P. Fang, S. Wang, P. Mary, R. Wang, P. Ma, R. Li, Y. Tian, Y. Cao, F. Li, L. Schweizer and H. Zhang, *Sci. Adv.*, 2021, **7**, eabe3839.
- 11 N. J. Martinez, S. A. Titus, A. K. Wagner and A. Simeonov, *Expert Opin. Drug Discovery*, 2015, **10**, 1347–1361.
- 12 Y. Endo, Y. Nakahara, R. Shiroma, K. Takimoto and Y. Matsuda, *Org. Process Res. Dev.*, 2024, **28**, 1806–1813.
- 13 Y. Yang, R. Rao, J. Valliere-Douglass and G. Tremintin, *J. Chromatogr. B*, 2024, **1235**, 124007.
- 14 A. Goyon, M. Kim, L. Dai, C. Cornell, F. Jacobson, D. Guillearme and C. Stella, *Anal. Chem.*, 2019, **91**, 14896–14903.
- 15 E. Ferraro, J. Z. Drago and S. Modi, *Breast Cancer Res.*, 2021, **23**, 84.
- 16 M. Abdollahpour-Alitappeh, M. Lotfinia, T. Gharibi, J. Mardaneh, B. Farhadihosseinabadi, P. Larki, B. Faghfourian, K. S. Sepehr, K. Abbaszadeh-Goudarzi, G. Abbaszadeh-Goudarzi, B. Johari, M. R. Zali and N. Bagheri, *J. Cell. Physiol.*, 2019, **234**, 5628–5642.
- 17 S. Andris, M. Wendeler, X. Wang and J. Hubbuch, *J. Biotechnol.*, 2018, **278**, 48–55.
- 18 J. Ouyang, in *Antibody-Drug Conjugates*, ed. L. Ducry, Humana Press, Totowa, NJ, 2013, pp. 275–283.
- 19 S. Fekete, J.-L. Veuthey, A. Beck and D. Guillearme, *J. Pharm. Biomed. Anal.*, 2016, **130**, 3–18.
- 20 M. Sarrut, A. Corgier, S. Fekete, D. Guillearme, D. Lascoux, M.-C. Janin-Bussat, A. Beck and S. Heinisch, *J. Chromatogr. B*, 2016, **1032**, 103–111.
- 21 M. Sarrut, S. Fekete, M.-C. Janin-Bussat, O. Colas, D. Guillearme, A. Beck and S. Heinisch, *J. Chromatogr. B*, 2016, **1032**, 91–102.
- 22 Y. Yan, T. Xing, S. Wang, T. J. Daly and N. Li, *J. Pharm. Biomed. Anal.*, 2020, **186**, 113313.
- 23 A. Wagh, H. Song, M. Zeng, L. Tao and T. K. Das, *mAbs*, 2018, **10**, 222–243.
- 24 Y. Chen, in *Antibody-Drug Conjugates*, ed. L. Ducry, Humana Press, Totowa, NJ, 2013, pp. 267–273.
- 25 V. Metrangolo and L. H. Engelholm, *Cancers*, 2024, **16**, 447.
- 26 Z. Tawfiq, Y. Matsuda, M. J. Alfonso, C. Clancy, V. Robles, M. Leung and B. A. Mendelsohn, *Anal. Sci.*, 2020, **36**, 871–875.

